Direct Hydrazine Fuel Cell Driven by a Non-bonded Cathodic Interface

A Thesis submitted to
Indian Institute of Science Education and Research Pune
in partial fulfilment of the requirements for the
BS-MS Dual Degree Programme
By

Mr. SWAPNIL VARHADE

Registration Number: 20131131

Supervisor: ***Dr. MUHAMMED MUSTHAFA***,
Assistant Professor, Department of Chemistry
Indian Institute of Science Education and Research Pune
Dr. Homi Bhabha Road, Pashan,
Pune 411008, INDIA.

Certificate

This is to certify that this dissertation entitled **"Direct hydrazine Fuel Cell Driven by a Non-Bonded Cathodic Interface"** towards the partial fulfilment of the BS-MS dual degree programme at the **Indian Institute of Science Education and Research, Pune** represents study/work carried out by **Swapnil Varhade (Reg. No. 20131131)** at Indian Institute of Science Education and Research Pune under the supervision of **Dr. Muhammed Musthafa O T, Assistant Professor, Department of Chemistry , IISER Pune** during the academic year 2017/2018.

Date: 20/3/2018
Place: Pune

Dr. Muhammed Musthafa O T,
Assistant Professor,
Department of Chemistry,
IISER Pune.

डॉ.मुहमद मुस्तफा/ Dr. Muhammed Musthafa
सहायक प्राध्यापक/ Assistant Professor
भारतीय विज्ञान शिक्षा एवं अनुसंधान संस्थान
Indian Institute of Science Education & Research
पुणे-411 008, भारत/ Pune - 411 008, India

Declaration

I hereby declare that the matter embodied in the report entitled **"Direct hydrazine Fuel Cell Driven by a Non-Bonded Cathodic Interface"** are the results of the work carried out by me at the **Department of Chemistry**, **IISER Pune**, under the supervision of **Dr. Muhammed Musthafa O T** and the same has not been submitted elsewhere for any other degree.

Varhade

Date: 20/3/2018

Place: Pune

Swapnil Varhade

(Reg. No.20131131)

Acknowledgements

First of all, I would like to express my heartfelt gratitude and sincere indebtedness to my supervisor ***Dr. Muhammed Musthafa O. T.***, Assistant Professor, Department of Chemistry IISER Pune for giving me this stupendous opportunity of doing the thesis project with him. His guidance and motivation whenever I needed it throughout the project had helped me to move in the right direction. I am able to complete this project because of his supervision.

I am thankful to ***Dr. P. A. Joy***, Chair, Physical and Materials Chemistry Division, NCL Pune for his continuous support throughout my project.

I would like thank specially to ***Zahid Bhat***, ***Alagar Raja, Mruthunjayachari C D, Dr. Ravikumar and Dr. Shahid Shafi*** who helped me a lot throughout the project. I am also grateful to ***Dr. Chidananda, Manu Gautam, Pramod Gaikwad, Soumodip Sur, Neetu C D, Mohammed Fawaz, Shambhulinga Aralekallu, Mahesh Itagi, Siddhi Khaire,*** and all other members who advised me in the project.

I am grateful to Ministry of Human Resource Development (MHRD), Government of India for providing the remarkable research facility under BS-MS program at IISER Pune.

I would like to thanks to all my friends in IISER Pune.

Finally, I want to express my very profound gratitude to my parents for providing me with unfailing support and continuous encouragement throughout my years of study.

Table of Content

List of Figures

Chapter 1. Introduction

Chapter 2. Experimental Section

Chapter 3. Results and Discussion

List of Tables

Chapter 3. Results and Discussion

ABSTRACT

Hydrazine is a toxic pollutant with high hydrogen content, offering tremendous possibilities in a direct hydrazine fuel cell (DHFC) as it can be converted into electricity via greener end products such as N_2 and H_2O. In state of the art hydrazine-air fuel cells since both half-cell chemistries are inner sphere, the Pt based air electrode often experiences unwanted competition and parasitic chemistry due to hydrazine cross over, overly complicating the already sluggish electrode kinetics at the positive electrode. Here we illustrate that by altering the interfacial chemistry of the positive electrode from inner sphere to outer sphere, the parasitic chemistry can be dissociated from the redox chemistry of the electron acceptor and the fuel cell can be driven by simple carbon-based cathodes. The DHFC-outer sphere fuel cell delivered an open circuit voltage of 1.3 V, a peak powder density of ~110 mW/cm^2 at a peak current density of ~200 mA/cm^2 which are almost 4 times higher than air breathing DHFC configuration.

CHAPTER 1. INTRODUCTION

From the last few decades, unconscionable use of non-renewable sources of energy is causing them to deplete at a faster rate than expected[1]. Combustion of these non-renewable resources causes the emission of harmful gases due to which 21st century is facing the problem of paramount pollution and anthropogenic global warming.[2-3] Exhausting fuel reservoirs and increasing environmental pollution drives people to find alternative sources of energy. Therefore, zero emission electrochemical conversion and storage technologies such as batteries, capacitors, solar cells and fuel cells are viable alternatives to address the impending calamities.[4-7] Although all of these systems have different ways to convert and store energy, they have one common feature that the energy providing process occur at the electrode electrolyte interface.

1.1 Battery

Battery is the electrical connection of one or more electrochemical cell. An electrochemical cell consists of anode (positive electrode) and cathode (negative electrode) separated by electrolyte. Charge transfer reactions happening near the electrode/electrolyte interface creates a potential difference between the anode and cathode.[8] Due to these potential differences, electrons flow from electrode having low reduction potential to the electrode having high reduction potential. So, the cell convert chemical energy to electrical energy during discharge chemistry and the process is reversed during charging chemistry.[9]

Battery is basically a chemical energy storage device which converts it into electrical energy only when it needed. Primary battery and secondary battery are two different categories of battery. Primary battery is the nonchargeable whereas secondary battery is chargeable[9]. Examples of primary batteries are zinc carbon and alkaline battery. Lithium ion battery, nickel metal hydride battery and lead acid battery are examples for secondary batteries.

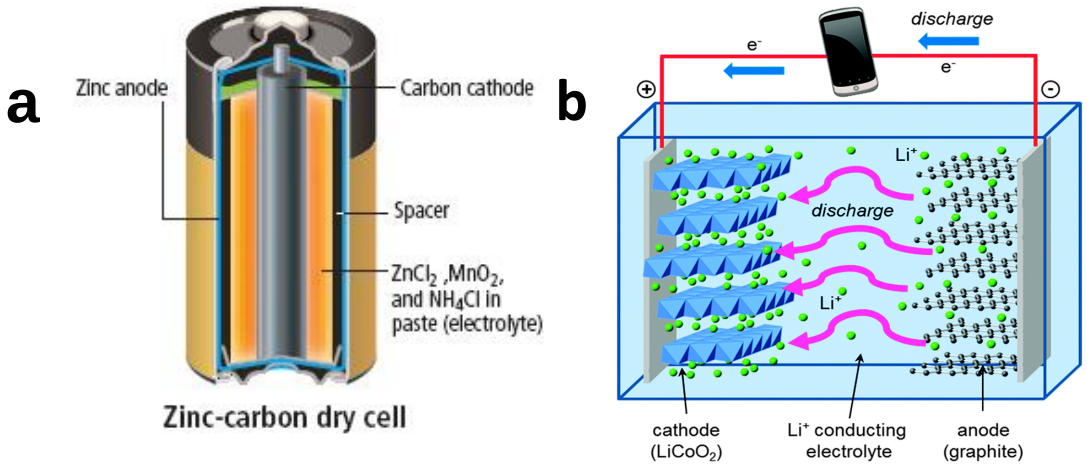

Figure 1.1: Schematics of (a) zinc-carbon battery and (b) Li-ion battery
a)(http://glencoe.mheducation.com/sites/007874637x/student_view0/chapter20/ section 2/self_check_quizzes.html#quest4
b)https://www.extremetech.com/extreme/212388-accidental- nanoparticles-could-let-lithium-ion-batteries-live-another-day)

1.2 Capacitor

Two conducting electrodes or metal plates separated by an insulating dielectric material form a capacitor. When a voltage is applied to a capacitor, there is collection of opposite charges on the surfaces of each electrode. The charges are kept separated with the help of dielectric material, thus producing an electric field. Due to little work done by external source and the electric field produced near the plates, energy is stored in the capacitor.[9] The two types of electrochemical supercapacitor are electrochemical double layer capacitors (EDLC) and pseudo capacitors. EDLC store charge with the help of adsorption of ion at the electrode/

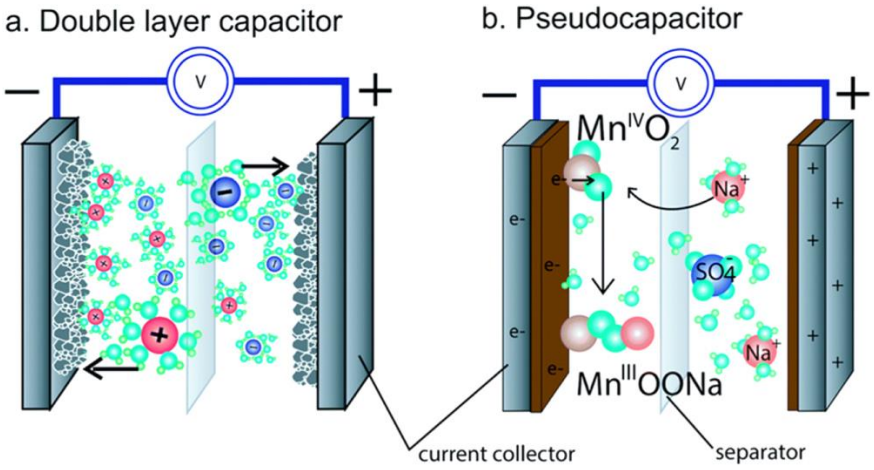

Figure 1.2: Schematics of (a) electrochemical double layer capacitor and (b) pseudo capacitor
http://iopscience.iop.org/article/10.1088/0957-4484/27/44/442001

electrolyte interface by non-faradic mechanism whereas pseudo capacitors store charge using fast redox reaction at the surface by faradic mechanism.[4,10]

1.3 Solar Cell

A solar cell is an electrical device that converts the light energy directly into electrical energy by the photovoltaic effect. The generation of current in a solar cell involves two key processes. The first process involves the creation of electron-hole pairs by absorption of incident photons. For the formation of electron-hole pairs in the solar cell, the energy of incident photons should be more than that of the band gap of the material used. A second procedure is the separation of carriers by the p-n junction to prevent their recombination.[11] They are separated by the electric field at the junction. Recombination of these carriers blocks the current generation.[11]

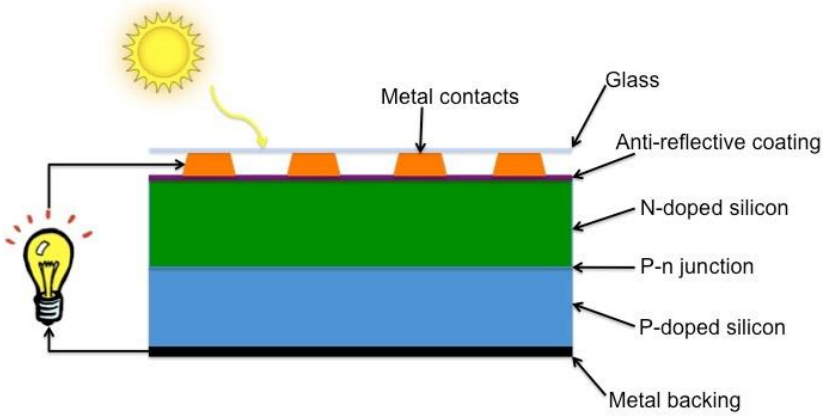

Figure 1.3: Scheme of a p-n junction solar cell
https://www.pinterest.se/pin/414401603183344889/

1.4 Fuel Cell

Fuel cell is an electrochemical conversion device in which two catalytic electrodes and an ion conducting membrane sandwiched to form membrane electrode assembly (MEA). Fuel is continuously supplied from both sides of the electrodes. The chemical energy from the fuel is getting converted to electrical energy. Just like a battery here also chemical reaction is happening at electrode electrolyte interface. But the major difference between battery and fuel cell is related to the location of energy conversion and storage. In fuel cell, the active mass taking part in the reaction is supplied from outside whereas in battery active mass is packed

inside the assembly. So, energy storage and conversion system are locally separated in the fuel cell.[9]

Proton exchange membrane fuel cell (PEMFC), solid oxide fuel cell, alkaline fuel cell, molten carbonate fuel cell etc are the different types of fuel cell.[12] Proton exchange membrane fuel cells (PEMFCs) are energy conversion devices at a higher efficiency with a near zero emission.[13-15] A proton exchange membrane fuel cell (PEMFC) converts the chemical energy of H_2 and O_2 into electricity, Figure 5. As shown in equations 1-3, H_2 enters the anodic compartment gets oxidised to form H^+ and the electrons released travel through external circuit to the cathode where it combines with O_2 and H^+ forming water.[16] State of the art PEMFC uses platinum based electrocatalysts to drive the reactions at the current density required.

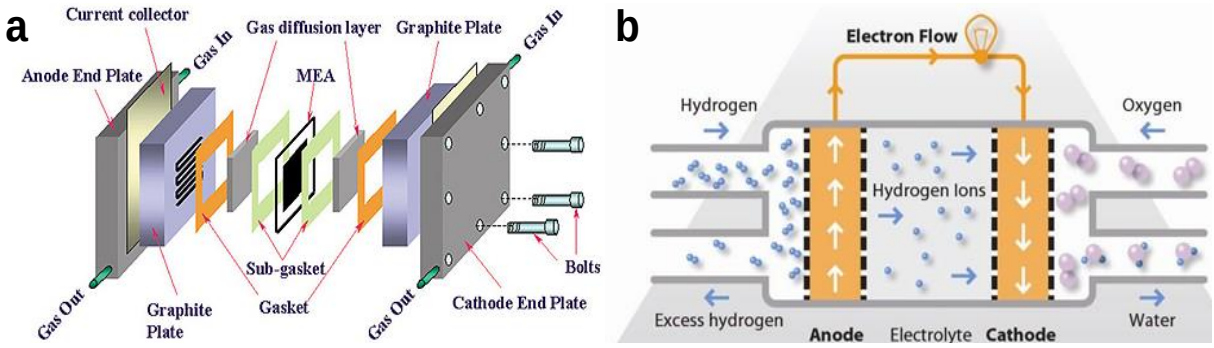

Figure 1.4: Scheme of a) fuel cell assembly and (b) a PEMFC
a) https://www.scientific-computing.com/feature/fuel-thought-cars-future
b) http://www.fuelcelltoday.com/technologies/pemfc

Oxidation reaction:

$$H_2 \longrightarrow 2H^+ + 2e^- \quad \text{..... Equation (1)}$$

Reduction Reaction:

$$O_2 + 4H^+ + 4e^- \longrightarrow 2H_2O \quad \text{..... Equation (2)}$$

Net Reaction:

$$2H_2 + 2O_2 \longrightarrow 2H_2O \quad \text{..... Equation (3)}$$

To overcome the safety and storage issues associated with explosive H_2 gas people have explored liquid fed fuel cells like direct alcohol fuel cell (DAFC), phosphoric acid fuel cell (PAFC), direct borohydride fuel cell (DBFC), etc.[17]

In the context of liquid fed fuel cells, direct hydrazine air fuel cells (DHAFC) have received significant attention due to the fact that a toxic pollutant can be converted into electricity in a non-toxic way.[18-20] Hydrazine is widely used in pharmaceutical industry, corrosion industry, as a catalyst in many chemical reactions and as an emulsifier.[21-22] However, it is a toxic pollutant often contaminating the water body and is carcinogenic and mutagenic in nature.[23-24] Therefore, in the context of fuel cells its conversion to electricity is particularly important and is fuelled by its liquid and non-carbonaceous nature.[25-26] Further, hydrazine a molecule rich with hydrogen and the oxidation of one molecule should generate 4 electrons with 1 molecule of nitrogen and 2 molecules of hydrogen.[26] But in DHAFC due to presence of OH^-, we get H_2O instead of H_2. DHAFC involves the oxidation of hydrazine at anode, equation 4 and reduction of oxygen molecule, equation 5 at cathode.[27]

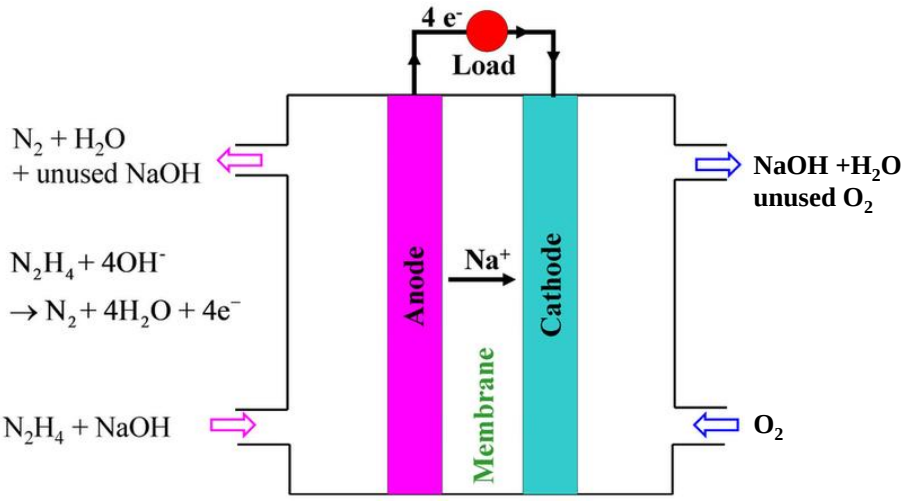

Figure 1.5: Schematic of hydrazine air fuel cell
https://www.researchgate.net/figure/Electrode-reactions-and-working-mechanism-of-the-DHHPFC_fig6_233893017

Oxidation reaction at anodic half cell:

$N_2H_4 + 4OH^- \longrightarrow N_2 + 4H_2O + 4e^-$ ..... Equation (4)

Reduction reaction at cathodic half cell:

$O_2 + 2H_2O + 4e^- \longrightarrow 4OH^-$ ..... Equation (5)

Net cell reaction:

$N_2H_4 + O_2 \longrightarrow N_2 + 2H_2O$ ..... Equation (6)

In the state of the art of direct hydrazine air fuel cell, the cathode always limits the overall performance.[28] Firstly, air reduction exhibits sluggish kinetics even on noble metal electrocatalyst and secondly the diffusion driven cross over of hydrazine to the cathode cause severe competition at cathodic sites.[25,29-30] Also, the carbon corrosion usually encountered in DHFC-O_2 fuel cell causes platinum electrode to degrade rapidly.[31-35] It is noteworthy to mention that since both half-cell chemistries are driven by Pt based electrocatalysts, these parasitic chemistries are triggered primarily by the inner sphere nature of electron transfer at either electrode. In diverse approach, we show a direct hydrazine fuel cell powered by an outer sphere electron acceptor that can undergo facile electron transfer even on simple carbon particles. Since the cathode is outer sphere, the diffusion driven cross over of hydrazine cannot evolve into a parasitic chemistry at the positive electrode, as carbon is kinetically inactive towards hydrazine, leading a DHFC-outer sphere fuel cell with performance metrics approximately 4 times higher than state of the art DHFC-air fuel cells.

CHAPTER 2. EXPERIMENTAL SECTION

2.1 Chemicals

Hydrazine hydrate (78-82%), H_2O_2 solution (30%), Potassium ferricyanide, Potassium hydroxide, Sulfuric acid, K_2HPO_4, KH_2PO_4, H_3PO_4, Acetic acid etc., were obtained from Sigma-Aldrich India. Pt/C was obtained from Johnson Matthey India. Ketjen black was obtained from fuel cell store(USA). Nafion@ 117 membrane was procured from Ion Power (USA).

2.2 Characterization techniques

Electrochemical measurements were done using the VMP300 Electrochemical Workstation (Biologic, France). The cleaning of all the working electrode was done with 0.05-micron alumina powder and then cycling the electrode in 0.5 M H_2SO_4.

a. Cyclic voltammetry

A cyclic voltammogram (CV) is the current vs potential curve of the response current recorded at the working electrode to the applied excitation potential across it.[36] CV is generally performed in three electrode configurations. The potential at the working electrode (WE) is monitored using a reference electrode (RE). The controlling potential applied

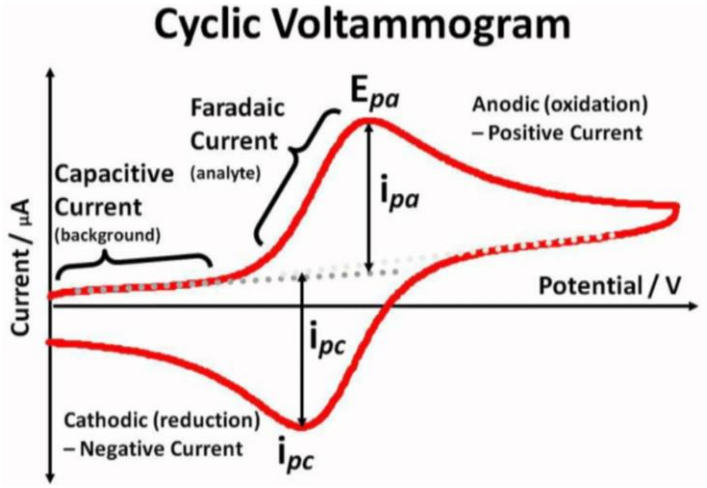

Figure 2.1: Schematic representation of cyclic voltammogram

https://www.youtube.com/watch?v=1f92vGOridg

across the WE and the counter electrodes is the excitation signal. The excitation signal shows linear variation with time at a specific sweep rate (in volts / second); first scan positively and then the potential is scanned in reverse direction, making a complete cycle hence the name cyclic voltammetry.[36] Cyclic voltammetry and linear scan voltammetry were done in standard three-electrode setup with a platinum (2 mm diameter) and glassy carbon (3 mm diameter) as working electrode, the counter electrode made of platinum mesh and an Ag/AgCl (3.5 M KCl) as reference. Hydrazine oxidation as well as crossover was studied using the platinum electrode while the redox behaviour of ferricyanide was studied using the glassy carbon electrode.

The number of electrons involved and peak potential difference in the CV of the redox reaction for a reversible couple is related by:

$$E_{pa} - E_{pc} = \frac{59mV}{n} \qquad \text{Equation (7)}$$

The relation of peak current in reversible systems with the scan rate is given by Randles-Sevcik equation[36],

$$I_{p_C} = (2.69 * 10^5) n^{3/2} A D^{1/2} \nu^{1/2} C \qquad \text{Equation (8)}$$

where, I_{pc} represents peak current (A), n shows number of electrons involved, A = electrode area (cm^2), D = diffusion coefficient (cm^2/s), C = concentration (mol/cm^3) and ν = scan rate (V/s).

If the slope of plot log peak current vs log scan rate comes out to be 0.5, then the process is considered as diffusion controlled. For surface-controlled process, the slope of the plot has to be 1.

b. Chronoamperometry

Chronoamperometry is technique in which constant potential is applied on working electrode and current is measure as a function of time using proper a reference electrode. For the irreversible processes, the difference of peak potentials in cyclic voltammetry widens. In irreversible systems, you cannot use Randles-Sevcik equation for extraction of parameters. In such cases, Cottrell equation is useful to calculate the diffusion coefficient.[37]

$$i(t) = \frac{nFACD^{1/2}}{(\pi t)^{1/2}}$$ Equation (9)

i =current (A), F=faraday constant, A=area of electrode (cm^2), C= concentration of solution ($moles/cm^3$), D=diffusion coefficient (cm^2/s), t=time (s)

c. Chronopotentiometry

Chronoamperometry is an important technique usually used for the electroplating where constant current is applied on the working electrode and potential of the electrode is monitored as a function of time using a reference electrode. Chronopotentiometry was used to coat the stainless steel electrode by platinum using the chloroplatinic acid for making the working electrode for the hydrazine oxidation.

d. Rotating Disk Electrode Study

Rotating disk electrode (RDE) studies (PAR instruments) were carried out in nitrogen purged solution of 1 mM hydrazine in 1 M KOH at 10 mV/s scan rate in a three-electrode system containing platinum disk electrode (0.196 cm^2) as working electrode, counter electrode made of platinum wire and Ag/AgCl (3.5 M KCl) as reference electrode at different RPM values (100, 400, 900, 1600, 2500, 3600, 4900, 6400). Number of electrons was calculated using the Koutecky-Levich equation,[38]

$$\frac{1}{j} = \frac{1}{j_k} + \frac{1}{j_l}$$ Equation (10)

where j is the total current density, j_k is kinetic current density and j_l is the limiting current density.

$$j_l = 0.62nFD^{2/3}\nu^{-1/6}C\omega^{\frac{1}{2}}$$ Equation (11)

$$\frac{1}{j} = \frac{1}{j_k} + \frac{\omega^{-1/2}}{0.62nFD^{2/3}\nu^{-1/6}C}$$ Equation (12)

where D (cm^2/s) is the diffusion constant, F means Faraday constant, ν is the kinematic viscosity (cm/s), n represents number of electrons, ω (radians/second) is the rotation rate and C ($moles/cm^3$) is the bulk concentration. The reciprocal of current density was plotted against reciprocal of rotation rates at different potentials.

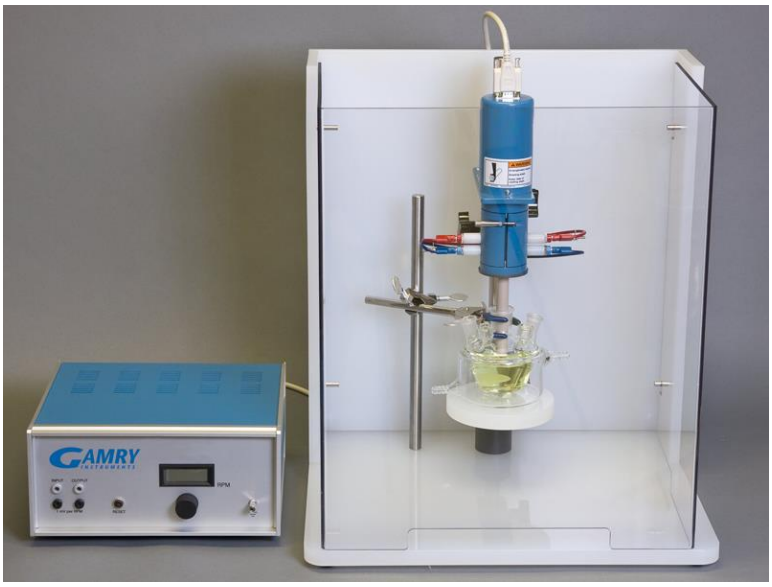

Figure 2.2: Pictorial representation of RDE instrument

https://www.gamry.com/cells-and-accessories/instrument-accessories/rde710-rotating-electrode/

From the slope of this plot equals $(0.62nFD^{2/3}v^{-1/6}C)^{-1}$, the number of electron involved in the reaction was estimated. The intercept of the plot of reciprocal of limiting current density vs. the reciprocal of rotation rates gives the reciprocal of kinetic current density. The kinetic current is related to overpotential as per the following relation,

$$j_k = k^0 CF\, exp[-\alpha nF(E - E^0)/RT] \qquad \text{Equation (13)}$$

where k^0 = heterogeneous rate constant (cm/s), C = bulk concentration (moles/cm^3), $E-E^0$ = overpotential, α= transfer coefficient. The rate constant and transfer coefficient was calculated by plotting overpotential against log of kinetic current density. The slope in the graph of overpotential against log of kinetic current density is equal to $2.303RT/\alpha nF$. The x-intercept of plot of over potential vs log kinetic current density is equal to the log of exchange current density from which k^0 was estimated.[38]

$$\frac{2.303RT}{\alpha nF} = \frac{d\eta}{d\, log\, j_k} \qquad \text{Equation (14)}$$

$$10^{-x} = FCk^0 \qquad \text{Equation (15)}$$

where, x = x intercept

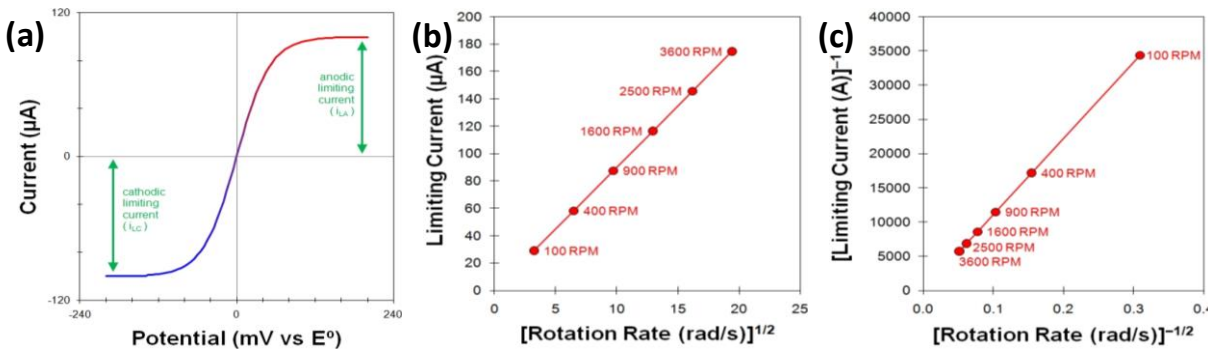

Figure 2.3: a) Voltammogram showing anodic and cathodic limiting current (b) Levich plot (c) Koutecky levich plot

https://www.pineresearch.com/shop/knowledgebase/rotating-electrode- theory/

e. Klinger Kochi and Nicholson method for heterogeneous rate constant calculation[39-40]

Both the methods are based upon peak potential difference with respect to scan rate.Nicholson method employs the relation between kinetic parameter (Ψ) with the rate constant (k°) which is given as,

$$\psi = k^0 \left[\frac{\pi D n v F}{RT}\right]^{-1/2} \qquad \text{Equation (16)}$$

Where D = diffusion coefficient (cm^2/s), n=number of electrons, R=universal gas constant, v = scan rate (V/s), F=Faraday constant and T= temperature (K). The kinetic parameter is deduced from the peak potential difference (ΔE) in the cyclic voltammetry. The function which fits the Nicholson data for the practical purpose is given by,

$$\Psi = \frac{-0.6228+0.0021\Delta E}{1-0.017\Delta E} \qquad \text{Equation (17)}$$

The slope of plot ψ against the $\nu^{-1/2}$ is equal to $k^0\left[\frac{\pi DnF}{RT}\right]^{-1/2}$. The heterogeneous rate constant can be calculated from the slope. Nicholson method is valid up to peak potential separation below 150 mV.[40]

Heterogeneous rate constant is calculated using Klinger and Kochi[39] method, when the potential difference between the peaks exceeds 200 mV.

According to this method the heterogeneous rate constant is given by the following relation,

$$k^0 = 2.18\left[\frac{D\beta nF\nu}{RT}\right]^{1/2} exp\left[\frac{\beta nF\Delta E}{RT}\right] \qquad \text{Equation (19)}$$

k^0=heterogenous rate constant (cm/s), β=transfer coefficient, ΔE=peak potential difference (V), ν = scan rate (V/s), n = number of electrons, R= universal gas constant, F= Faraday constant and T= temperature (K)

The value of transfer coefficient is calculated from the slope of the graph of peak potential against log of scan rate

$$\beta = \left[\frac{2.303RT}{2nF}\right]\left[\frac{dE_p}{d\log\nu}\right]^{-1} \qquad \text{Equation (18)}$$

β=transfer coefficient, E_p=peak potential (V), ν=scan rate (V/s), R=universal gas constant, n=number of electrons, T= temperature(K) and F=Faraday constant

f. Spectro electrochemistry

Spectro electrochemistry is the combination of electrochemistry with spectroscopy. In Spectro electrochemistry, electrochemical as well as optical process is monitored simultaneously. The in-situ Spectro electrochemical data (UV-Vis) for potassium ferricyanide (1 mM) in 1M KOH is collected using the three-electrode system. Hg/HgO (1M NaOH) electrode was used as a reference electrode, platinum wire was used as counter electrode and platinum mesh was used as working electrode.

g. Infrared spectroscopy

IR spectroscopy, name itself is self-explanatory. Spectroscopy means the study of interaction of light with matter. So, IR spectroscopy is the study of interaction of infrared light with the molecules. Vibrational motion of molecules plays important role in IR spectroscopy. According to the several different vibrational

motions, molecules will absorb IR radiation of varying intensity at different IR frequencies.[41] Thus, different chemical bond and functional group will absorb radiation at different frequencies. Therefore, IR spectroscopy is useful to detect or distinguish a particular kind of bond or functional group.

FTIR spectroscopy is used to show that whether the carbon corrosion is degrading the platinum electrode during the galvanostatic study of fuel cell.

ATR-FTIR (Bruker Alpha FTIR Spectrometer System) is used to collect the FTIR data.

h. Ultra-violet visible spectroscopy

UV visible spectroscopy is the type of molecular spectroscopy in which ultra violet, visible radiation interacts with molecules. When radiation is incident on molecule, it will absorb a radiation of particular wavelength. Absorption of light will cause the transition of electron from filled molecular orbital to the higher energy unfilled molecular orbital. The transition of electron is generally takes place in electronic energy levels. [42] The information about energy gap related to functional group can be obtained from the wavelength of absorbed light.

According to Beer Lambert law, absorption is proportional to concentration of molecules and path length of light through tube

$$\boldsymbol{A = \varepsilon C l} \qquad \text{Equation (20)}$$

where A = absorbance, ε = molar absorptivity ($mol^{-1}cm^{-1}$), C=concentration of molecule (mol /L)

UV visible spectroscopy was used to collect the UV-Vis spectra of Fe^{2+} and Fe^{3+}.

UV-3600 Plus UV-VIS-NIR spectrophotometer was used to collect the data.

2.3 Fuel Cell assembly

Pre-treatment of Nafion membrane: A Nafion@117 membrane were pre-treated with the H_2O_2 and water solution taken in 1:3 ratio, respectively. This solution is heated at 80^0C for 30 minutes. After washing with distilled water, Nafion membrane is again heated at 80^0C for 30 minutes in H_2SO_4 solution.[43]

DHFC-O_2 fuel cell was assembled with Pt/C based electrodes on both side. The Pt/C catalyst ink was made by mixing Pt/C (1 mg of Pt per cm^2), isopropanol and 10 wt% PTFE binder and sonicating it for 30 minutes. The resulting ink was sprayed on to Toray carbon paper. A pre-treated Nafion@117 membrane was used between the two electrodes and the whole setup was placed between the graphite plates. 3 M Hydrazine in 1 M KOH was used from anodic compartment with flow rate of 100 mL/minute and humidified O_2 was continuously supplied at a flow rate of 0.25 slpm.

DHFC-outer sphere fuel cell was assembled as follows. The anode electrode was fabricated by coating the catalyst i.e. Pt/C (60 wt% Pt) on Toray carbon paper with 0.5 mg/cm^2 loading. Similarly, for the cathode, Ketjen black carbon nanoparticles were used in place of Pt/C. The catalyst inks were prepared by scattering known amounts of Ketjen black (10 wt% of PTFE binder) and Pt/C (10 wt% of Nafion@ binder) in isopropanol by sonication for about 30 minutes. A pre-treated Nafion@ 117 membranes were used between the two electrodes and the whole setup was placed between the graphite plates having inlets and outlets for the flowing solutions. 3 M Hydrazine in 1 M KOH was used from anodic compartment and 1 M potassium ferricyanide in 1 M KOH was used from cathodic compartment. The flow rate from both the side is 100mL/minute.

CHAPTER 3. RESULTS AND DISCUSSION

The scheme of the DHFC outer sphere fuel cell (scheme 1) suggests that it consist of an anodic compartment containing hydrazine in alkali and a cathodic compartment containing an alkaline solution of outer sphere electron transfer agent such as ferricyanide separated by a Nafion@117 membrane. Anodic electrocatalyst was Pt and cathodic current collector was carbon particles deposited on a Toray carbon paper. Pt is the benchmark electrocatalyst for hydrazine oxidation in alkaline media.[44-46]

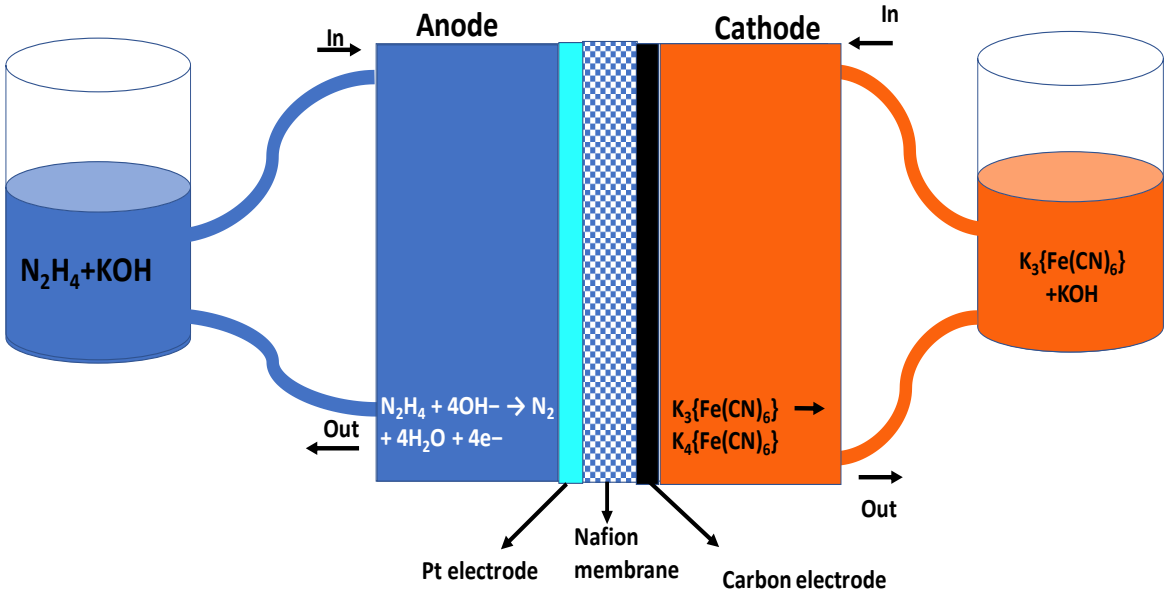

Scheme 3.1: Schematics of DHFC outer sphere fuel cell.

3.1 Anodic Chemistry

The linear scan voltammogram of hydrazine oxidation on platinum and glassy carbon electrode shows that glassy carbon is inactive toward hydrazine oxidation, Figure 3.2a. Therefore, the platinum electrode is used to collect the scan rate dependence study of hydrazine oxidation, figure 3.2b. The curve peak current against square root of scan rate shows linearity, figure 3.2c. The slope of the curve log (peak current) against log scan rate is near 0.5, Figure 3.2d. This shows that the process is diffusion-controlled. The rotating disk electrode (RDE) studies and Koutecky Levich plot indicate the numbers of electrons transferred are close to 4,

Figure 3.3a and 3.3b suggesting the anodic half-cell chemistry is the oxidation of hydrazine into N_2 and H_2O as demonstrated in equation 21

$$N_2H_4 + 4KOH \rightarrow N_2 + 4H_2O + 4e^- + 4K^+ \qquad \text{Equation (21)}$$

The rate constant for the reaction is ~1.7×10^{-3} cm/s from RDE measurements, Figure 3.3c, Table 3.1. The diffusion coefficient of hydrazine was calculated using Randles-Sevcik equation and Cottrell equation, Figure 3.3d, Table 3.2. All these suggest that Pt is a decent catalyst for the 4 electron oxidation of hydrazine.

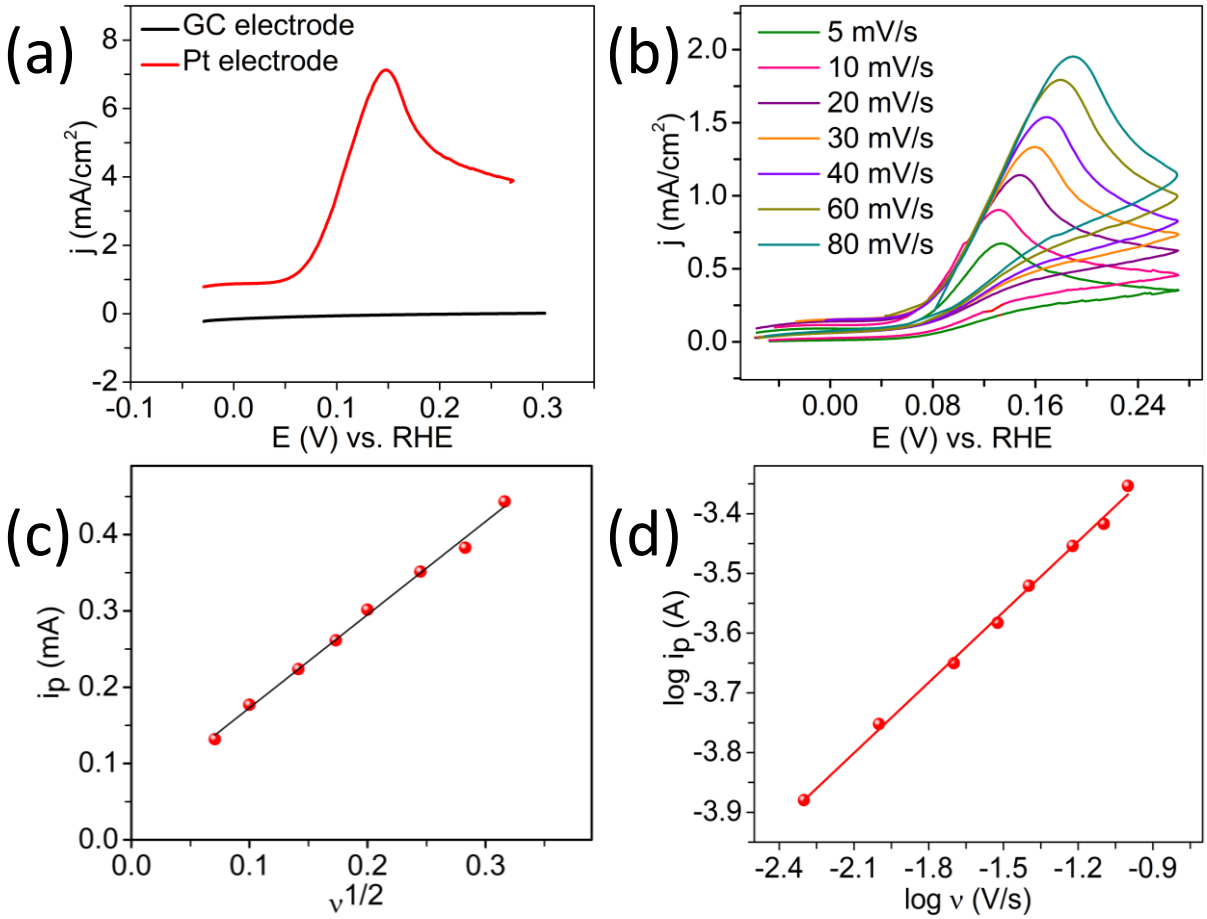

Figure 3.2: (a) Linear sweep voltammograms for the oxidation of 10 mM hydrazine (in 1 M KOH) on a carbon as well as a platinum electrode, (b) cyclic voltammograms for the oxidation of 1 mM hydrazine in 1 M KOH on platinum electrode at different scan rate, (c) plot of peak current against square root of scan rate and (d) plot of log of peak currents versus log of scan rates.

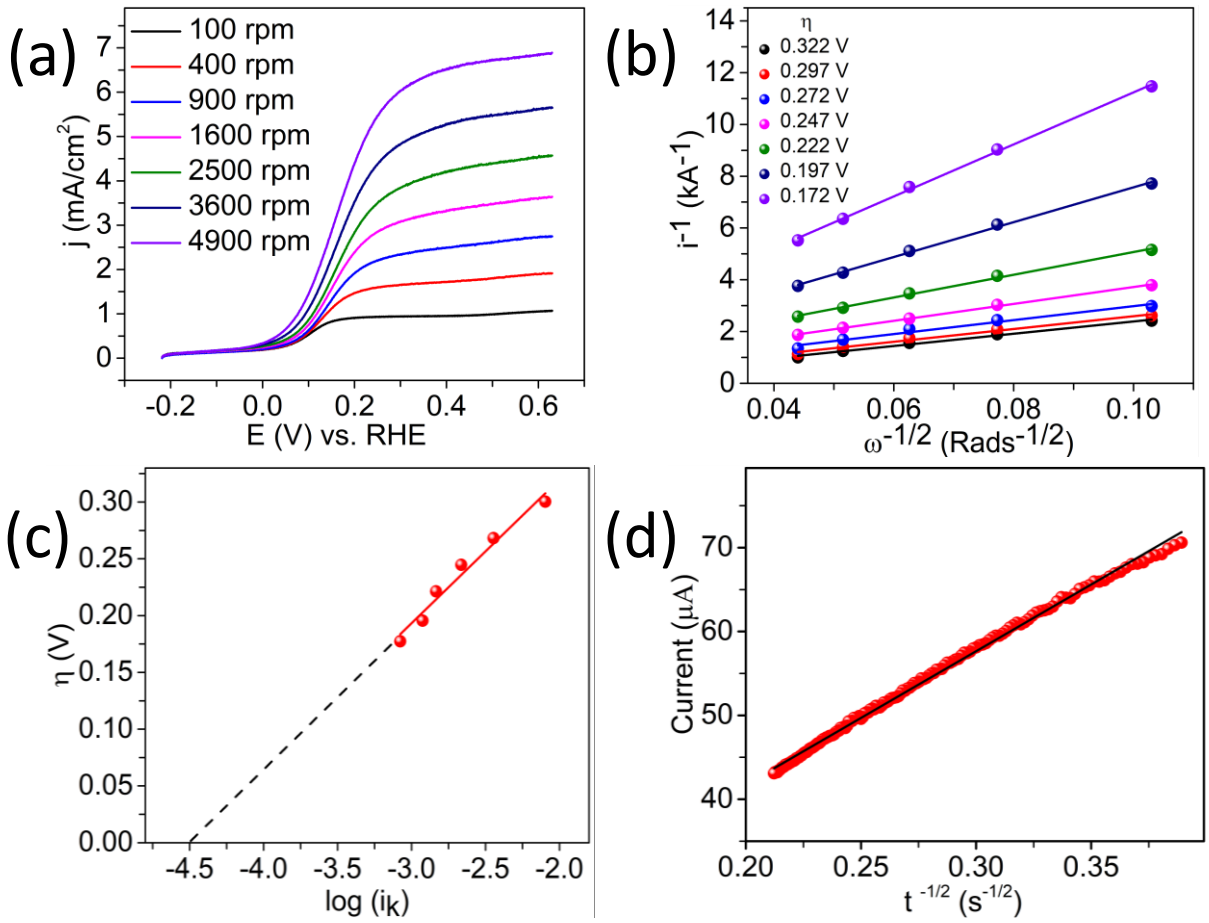

Figure 3.3: (a) Rotating disk electrode (RDE) measurements acquired on a platinum electrode for the oxidation of 1 mM hydrazine at various rotation rates, (b) Koutecky−Levich plots at different overpotential, (c) overpotential vs. log of kinetic current for the calculation of rate constant and (d) Cottrell plots for hydrazine oxidation.

Table 3.1: Parameters extracted from RDE experiment for hydrazine oxidation on a Pt electrode.

Parameters	Values
Number of electron (n)	4
Transfer coefficient (α)	0.117
Rate constant (k)	1.67 X 10^{-3} cm/s

Table 3.2: Diffusion coefficient for hydrazine oxidation on a Pt electrode.

Method	Diffusion Coefficient (cm^2/s)
Randles Sevcik Equation	2.8 X 10^{-6}
Cottrell Equation	4.6 X 10^{-6}

3.2 Cathodic Chemistry

The cathodic counterpart, ferricyanide, undergoes fast and effortless electron transfer even on carbon electrode due to its outer sphere nature, Figure 3.4a and 3.4b. ½ slope for the log (peak current) vs. log (scan rate), figure 3.4c. indicates a diffusion-controlled process. This is further supported by linearity of the plot of peak current vs. concentration Figure 3.4d. RDE studies further indicate the number of electrons transferred are close to 1, Figure 3.5a, Table 3.3 and the rate constant on simple carbon electrode ~3.3×10^{-2} cm/s from RDE measurements, Figure 3.5b and Figure 3.5c suggesting a relatively fast redox reaction. Klinger Kochi and Nicholson's method, Figure 3.6a, 3.6b and 3.6c, further reinforce that the rate constants are in the same order on carbon-based electrode materials, Table 3.4 and Table 3.5.

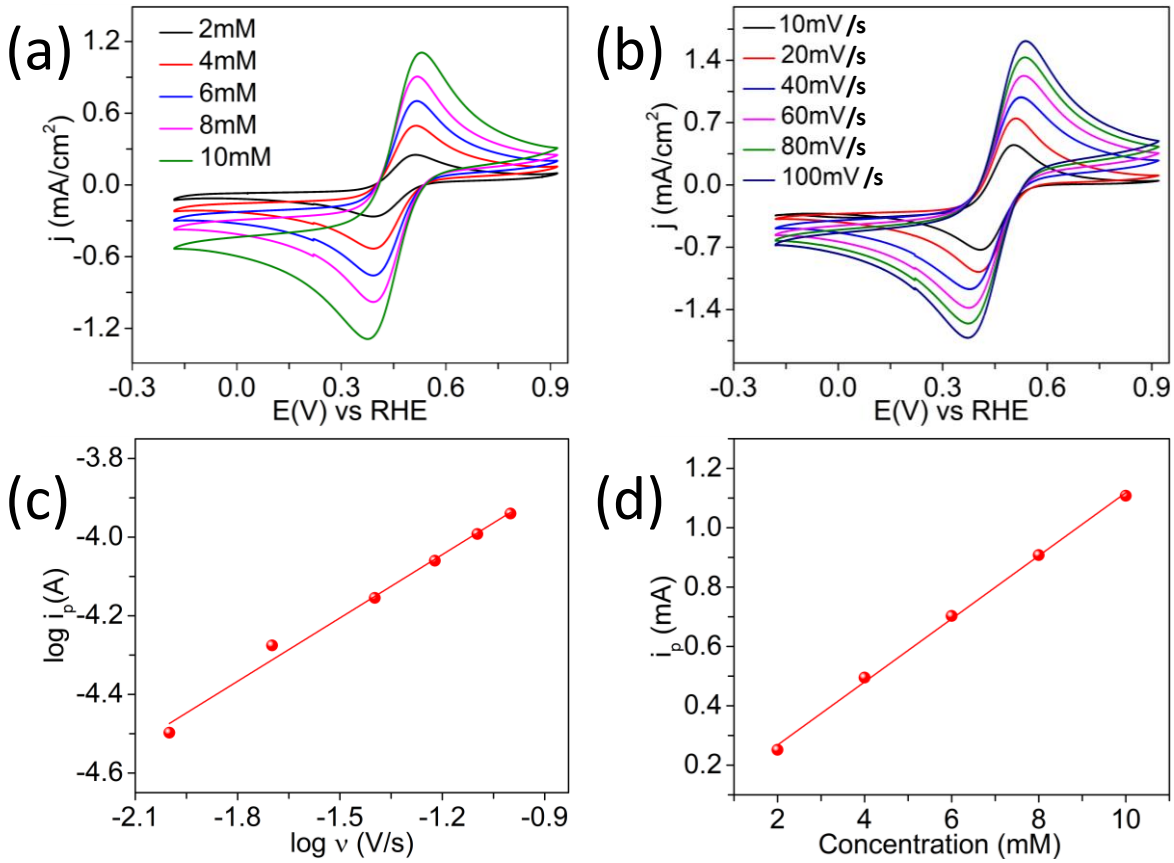

Figure 3.4: Cyclic voltammograms for ferricyanide (1 mM) in 1 M KOH at different (a) concentration and (b) scan rates on a glassy carbon electrode. (c) Plot of log of peak currents vs. log of scan rates and (d) plot of peak currents vs. concentration.

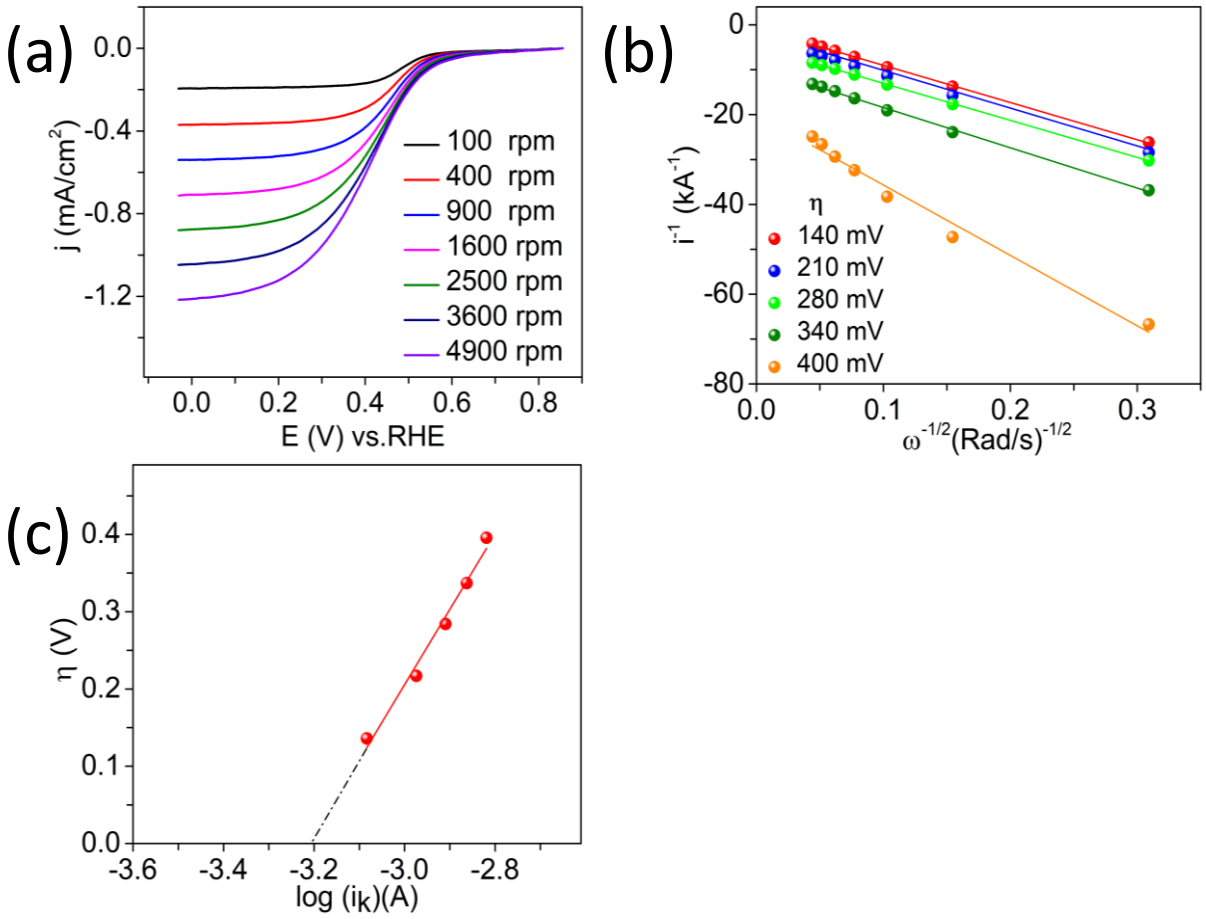

Figure 3.5: (a) Rotating disk electrode (RDE) measurements acquired on a glassy carbon electrode for ferricyanide (1 mM) in 1 M KOH at various rotation rates, (b) Koutecky−Levich plots at different overpotentials and (c) overpotential vs. log of kinetic current for the calculation of intrinsic rate constant.

Table 3.3: Parameters extracted from the RDE experiment for ferricyanide reduction on a carbon electrode.

Parameters	Values
Number of electron (n)	1
Symmetry factor (β)	0.29
Rate constant (k)	3.33 X 10^{-2} cm/s

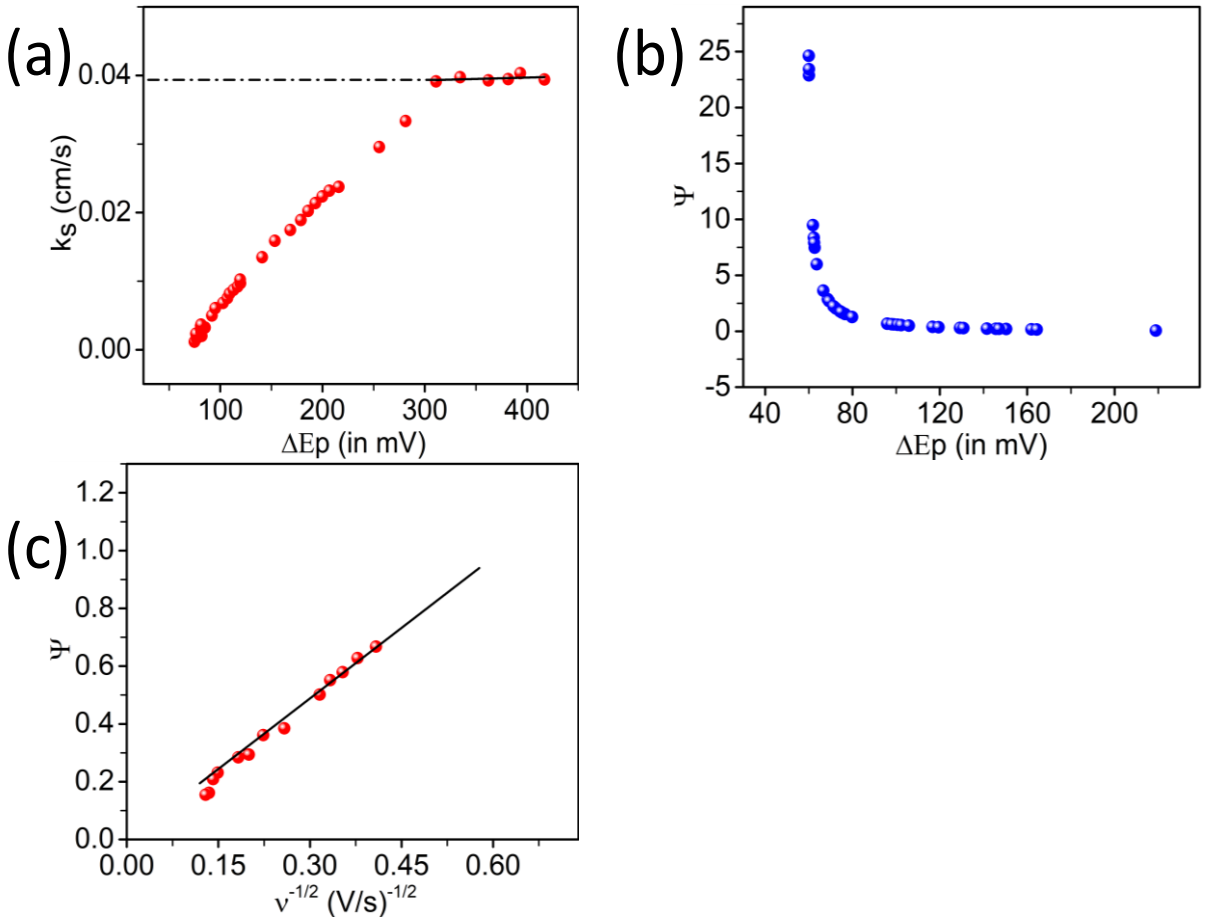

Figure 3.6: (a) Plot of change of heterogeneous rate constant with peak potential as per Klinger and Kochi method, (b) plot of kinetic parameter with peak potential difference and (c) plot of kinetic parameter against square root of scan rate to calculate heterogeneous rate constant by Nicholson method.

Table 3.4: Rate constant calculated from different methods for the redox reaction of ferricyanide on a carbon electrode.

Method	Rate Constant Values
RDE	3.33 X 10^{-2} cm/s
Klinger and Kochi	4 X 10^{-2} cm/s
Nicholson	2.4 X 10^{-2} cm/s

Table 3.5: Parameters calculated from Klinger-Kochi and Nicholson method.

ν (V/s)	ΔE (mV)	K (cm/s)
0.01	74.89	0.001
0.02	76.91	0.002
0.03	82.03	0.002
0.04	76.38	0.002
0.05	81.45	0.003
0.06	81.44	0.003
0.07	81.00	0.003
0.08	85.15	0.003
0.09	80.90	0.003
0.1	81.33	0.004
0.2	91.93	0.005
0.3	95.11	0.006
0.4	102.78	0.007
0.5	107.05	0.008
0.6	109.23	0.008
0.7	113.10	0.009
0.8	117.07	0.009
0.9	119.70	0.010
1	119.50	0.010
2	141.09	0.013
3	153.40	0.016
4	168.63	0.017
5	178.92	0.019
6	185.96	0.020
7	193.08	0.021
8	199.77	0.022
9	206.75	0.023
10	215.83	0.024
20	255.53	0.030
30	281.25	0.033
40	328.86	0.033
50	311.07	0.039
60	334.56	0.040
70	362.21	0.039
80	381.61	0.039
90	393.22	0.040
100	416.94	0.039

ν (V/s)	$(\gamma)^{-1/2}$	ΔE (mV)	Ψ
0.01	10	74.89	1.705
0.02	7.1	76.91	1.501
0.03	5.8	82.03	1.142
0.04	5	76.38	1.550
0.05	4.5	81.45	1.175
0.06	4.1	81.44	1.175
0.07	3.8	81.00	1.201
0.08	3.5	85.15	0.992
0.09	3.3	80.90	1.207
0.1	3.2	81.33	1.181
0.2	2.2	91.931	0.764
0.3	1.8	95.111	0.686
0.4	1.6	102.78	0.545
0.5	1.4	107.05	0.485
0.6	1.3	109.23	0.459
0.7	1.2	113.10	0.418
0.8	1.1	117.07	0.381
0.9	1.1	119.7	0.359
1	1	119.50	0.361
2	0.71	141.09	0.233
3	0.58	153.40	0.187
4	0.5	168.63	0.144
5	0.4	178.92	0.121
6	0.4	185.96	0.107
7	0.4	193.08	0.095
8	0.4	199.77	0.085
9	0.3	206.75	0.075
10	0.3	215.83	0.064
20	0.2	255.53	0.026
30	0.2	281.25	0.009
40	0.2	328.86	-0.015
50	0.1	311.07	-0.007
60	0.1	334.56	-0.017
70	0.1	362.21	-0.027
80	0.1	381.61	-0.033
90	0.1	393.22	-0.036
100	0.1	416.94	-0.042

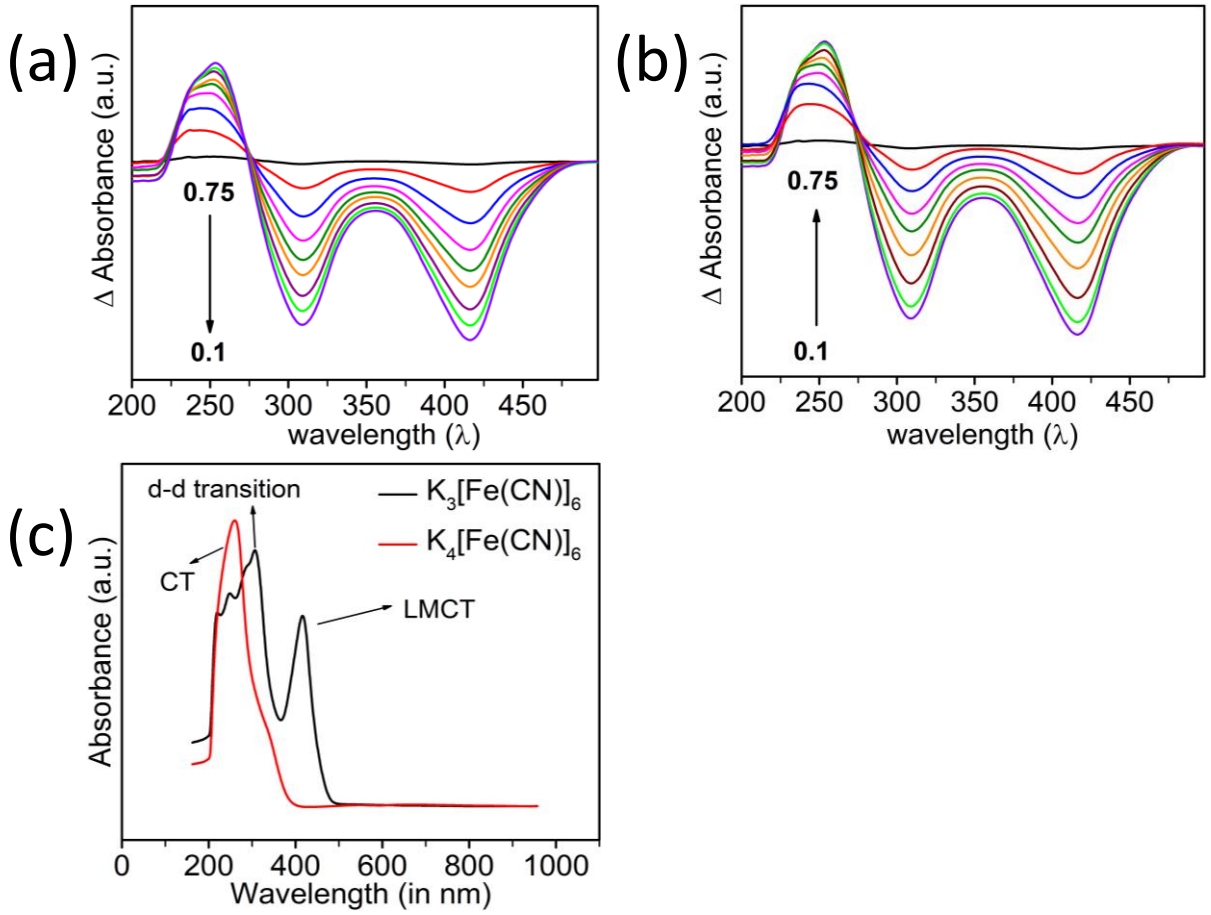

Figure 3.7: In-situ spectroelectrochemical data for ferricyanide (1 mM) in 1 M KOH during (a) reduction and (b) oxidation scans. (c) UV-visible spectra of ferrocyanide and ferricyanide complexes.

Therefore, ferricyanide redox reaction involves simple electron transfer without significant changes in atom to atom bonding. Spectroelectrochemistry and UV spectroscopy data suggest the reduction involves the formation of ferrocyanide and oxidation the regeneration of ferricyanide, Figure 3.7a, 3.7b and 3.8c. From the UV-Vis spectra of ferricyanide and ferrocyanide, it can be seen that ferricyanide has two major peaks so the two peaks (downside) in the in-situ UV-Vis spectra correspond to change of concentration of ferricyanide. The one which is increasing above is due to ferrocyanide. Both $[Fe\ (CN)_6]^{3-}$ and $[Fe(CN)_6]^{4-}$ have octahedral (Oh) symmetry. But the ferric centre has higher oxidation state than that of ferro and also it has vacancy in the ligand-field low-spin t_{2g} level. This makes ferric species different from ferrous. The ferrous species shows charge transfer to solvent (CTTS) band in the UV-Vis spectral region, but the ferric complex does not show this transition.[47]

Fe^{3+} is d5 system (therefore this system will be prone to Jahn-Teller distortion).Since CN^- is strong field ligand, $[Fe(CN)_6]^{3-}$ is a low spin complex. Due to Jahn-Teller distortion, there will be further splitting of t_2g and e_g orbitals according to the compression or elongation. Our system is d5 system so we don't know whether it will be elongation or compression. But even though there is elongation or compression, it does not matter here. So here two transitions are possible. Along with this there will be ligand to metal charge transfer (LMCT).[48] Due to LMCT, peak will be near UV region or at the starting of visible range. Fe^{2+} is a d6 system therefore it does not exhibit Jahn-Teller distortion as there is no degeneracy possible. There will be only charge transfer which will appear in the UV region.

Based on above discussed all studies, equation 22 is proposed for cathodic half-cell chemistry.

$K_3[Fe(CN)_6] + K^+ + 1e^- \rightarrow K_4[Fe(CN)_6]$ Equation (22)

3.3 Fuel Cell Performance

The single electrode potentials for hydrazine on a Pt electrode and ferricyanide on a carbon electrode, Figure 3.8a, suggest that hydrazine can be an electron donor and ferricyanide can plays the role of a strong electron acceptor with the net cell reaction (equation 23) being the oxidation of hydrazine at the anode(equation 23) and reduction of ferricyanide at the cathode (equation 22). Such a fuel cell delivered an OCV of ~1.3 V, a peak power density of ~110 mW/cm^2 at a peak current density of ~200 mA/cm^2, Figure 3.8b which is approximately 4 times higher than DHFC-O_2 fuel cells. The long-term polarization, Figure 3.8c suggests the DHFC outer sphere can sustain comparatively higher rates than DHFC-O_2 fuel cells. It further suggests that the energy density of DHFC-outer sphere fuel cell is almost four times higher compared to DHFC-O_2. Further the carbon corrosion usually encountered in DHFC-O_2 fuel cell, Figure 3.8d is not encountered in DHFC-outer sphere configuration. This could be due to absence of Pt and air in DHFC-outer sphere fuel cells as Pt is known to accelerate carbon corrosion in presence of air.32-36 We note that the performance of DHFC-air fuel cell can be improved by increasing the Pt loading and the back pressure of O2; however, these will have significant cost implications. We have further investigated the parasitic chemistry at

the cathode by monitoring the signals of hydrazine at the cathode as function of time, Figure 3.9a.

Net cell reaction:

$N_2H_4 + 4KOH + 4K_3 [Fe (CN)_6] \rightarrow N_2 + 4H_2O + 4K_4 [Fe (CN)_6]$ Equation (23)

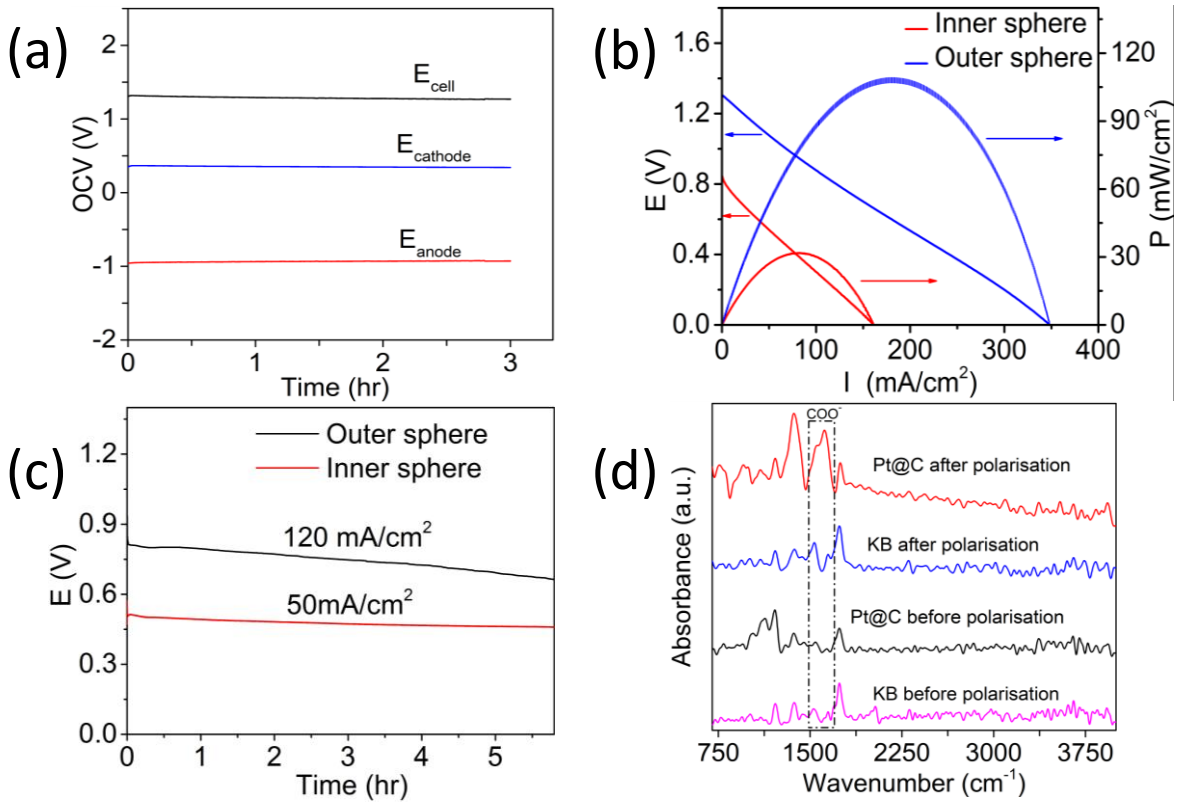

Figure 3.8: (a) Open circuit voltage vs. time plot, (b) polarization curves for DHFC−outer sphere fuel cell and DHFC-O_2 fuel cell. For the DHFC-outer sphere fuel cell, anode electrolyte is 3 M hydrazine in 1 M KOH and cathode electrolyte is 1 M potassium ferricyanide in 1 M KOH and flow rate is 100 ml/min. Loading of Pt on anode is 0.2 mg/cm^2 and loading of carbon on cathode is 3 mg/cm^2. For the DHFC-O_2 fuel cell, anode electrolyte is 3 M hydrazine in 1 M KOH and cathode is O_2 saturated 1 M KOH at flow rate of 100 ml/min. Loading of Pt on anode is 0.2 mg/cm^2 and loading of Pt on cathode is 0.5 mg/cm^2. (c) Galvanostatic polarization curves for DHFC-outer sphere and DHFC-O_2 fuel cells and (d) FTIR spectra of the cathode before and after long term stability tests.

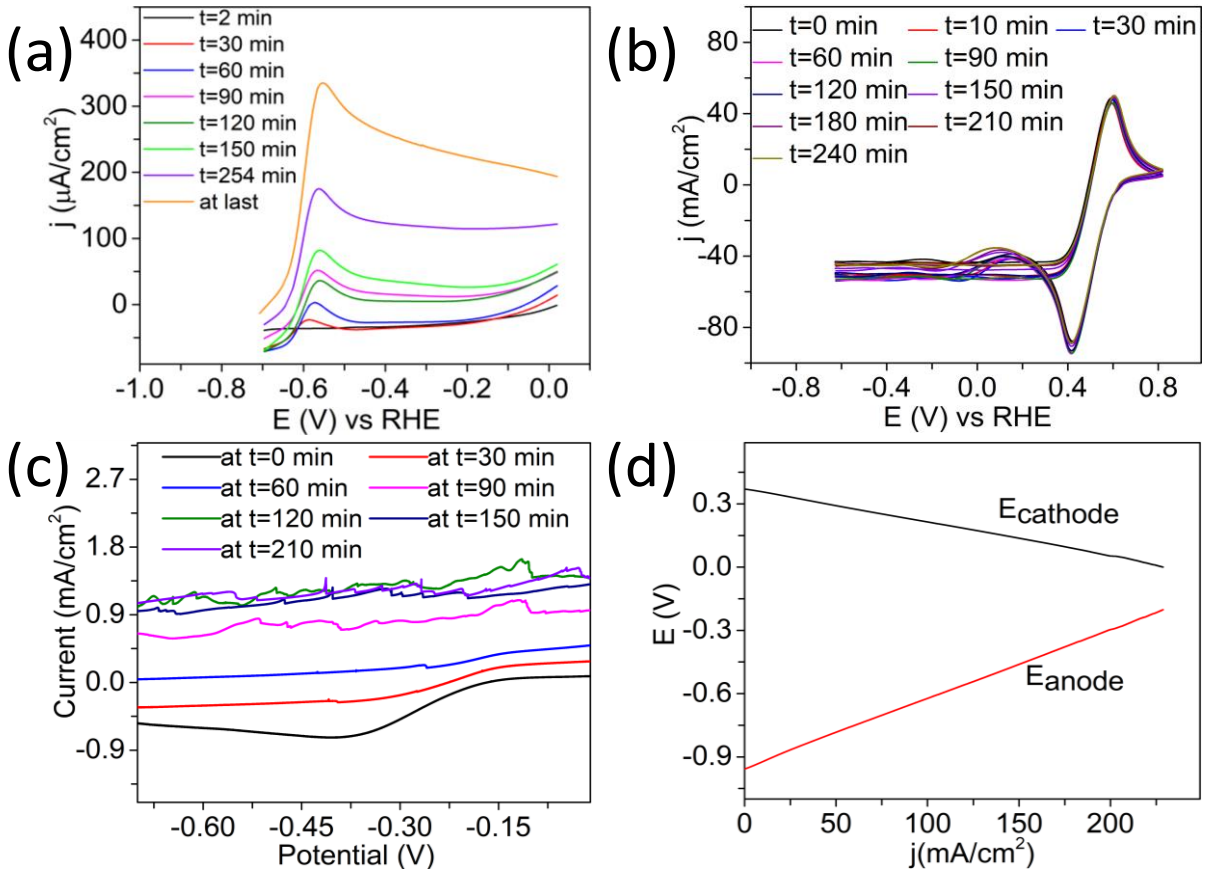

Figure 3.9: Cyclic voltammogram for time dependent crossover of hydrazine in (a) DHFC-O_2 fuel cell and (b) DHFC outer sphere fuel cell using cathode as the working electrode. (c) The effect of hydrazine crossover on oxygen reduction reaction in DHFC-O_2 fuel cell and (d) individual electrode polarization for DHFC outer sphere fuel cell.

Most importantly it can be seen the ORR peaks gradually disappears with a concomitant increase in cross over current from hydrazine in DHFC-O_2 fuel cells, however the ferricyanide redox reaction remain unchanged and hydrazine signals are absent in DHFC-outer sphere fuel cell, Figure 3.9b and Figure 3.9c. These suggest carbon is kinetically inert towards hydrazine oxidation and ferricyanide redox reaction remains unchanged irrespective of the presence of hydrazine in cathodic compartment, demonstrating parasitic chemistry can be effectively decoupled from the redox chemistry of electron acceptor. A comparison of individual polarization in DHFC-outer sphere, Figure 6c, suggests that the anode limit the overall performance of the fuel cell.

CHAPTER 4. CONCLUSIONS AND FUTURE OUTLOOK

We have shown a DHFC-outer sphere fuel cell driven by simple carbon particles with performance metrics of about 4 times higher than corresponding Pt based DHFC-O_2. This outer sphere fuel cell is able to arrest and decouple the parasitic chemistry triggered by hydrazine cross over from the redox chemistry of electron acceptor with energy density four times higher than state of the art DHFC-O_2 fuel cells. Platinum is an expensive metal, therefore it should be substituted by a non-precious electrocatalyst on the anode side as well to have a precious metal free DHFC. This aspect is a matter of future investigation. Our preliminary investigation suggests iron based molecular electrocatalyst anchored on carbon nanotube by pi-pi interaction can catalyse 4 electron oxidation of hydrazine. This molecular electrocatalyst for hydrazine oxidation on coupling with outer sphere redox electron acceptor is expected to reduce the cost of electricity/kW substantially from a DHFC.

REFERENCES

(1) Mourad, E.; Coustan, L.; Lannelongue, P.; Zigah, D.; Mehdi, A.; Vioux, A.; Freunberger, S. A.; Favier, F.; Fontaine, O. Biredox Ionic Liquids with Solid-like Redox Density in the Liquid State for High-Energy Supercapacitors. *Nat. Mater.* **2016**, *16* (November 2016).

(2) Larcher, D.; Tarascon, J. M. Towards Greener and More Sustainable Batteries for Electrical Energy Storage. *Nat. Chem.* **2015**, *7* (1), 19–29.

(3) Poizot, P.; Dolhem, F. Clean Energy New Deal for a Sustainable World: From Non-CO2 Generating Energy Sources to Greener Electrochemical Storage Devices. *Energy Environ. Sci.* **2011**, *4* (6), 2003.

(4) Chandran, P.; Ghosh, A.; Ramaprabhu, S. High-Performance Platinum-Free Oxygen Reduction Reaction and Hydrogen Oxidation Reaction Catalyst in Polymer Electrolyte Membrane Fuel Cell. *Sci. Rep.* **2018**, *8* (1), 3591.

(5) Miroshnikov, M.; Divya, K. P.; Babu, G.; Meiyazhagan, A.; Reddy Arava, L. M.; Ajayan, P. M.; John, G. Power from Nature: Designing Green Battery Materials from Electroactive Quinone Derivatives and Organic Polymers. *J. Mater. Chem. A* **2016**, *4* (32), 12370–12386.

(6) Feng, B.; An, H.; Tan, E. Screening of CO2 Adsorbing Materials for Zero Emission Power Generation Systems. *Energy and Fuels* **2007**, *21* (2), 426–434.

(7) Licht, S. STEP (Solar Thermal Electrochemical Photo) Generation of Energetic Molecules: A Solar Chemical Process to End Anthropogenic Global Warming. *J. Phys. Chem. C* **2009**, *113* (36), 16283–16292.

(8) Characteristics, C. Chapter 2 Electrode / Electrol Yte Interfaces: Structure and. **1900**.

(9) Principle, T. W.; Cell, S. The Working Principle of a Solar Cell. **1921**, *1*, 21–24.

(10) Conway, B. E.; Pell, W. G. Double-Layer and Pseudocapacitance Types of Electrochemical Capacitors and Their Applications to the Development of Hybrid Devices. *J. Solid State Electrochem.* **2003**, *7* (9), 637–644.

(11) Winter, M.; Brodd, R. J. What Are Batteries, Fuel Cells, and Supercapacitors? *Chem. Rev.* **2004**, *104* (10), 4245–4269.

(12) FuelCellToday(http://www.fuelcelltoday.com/). Fuel Cell Basics. **2012**.

(13) Therdthianwong, A.; Saenwiset, P.; Therdthianwong, S. Cathode Catalyst Layer Design for Proton Exchange Membrane Fuel Cells. *Fuel* **2012**, *91* (1), 192–199.

(14) Hsieh, C. Y.; Nguyen, X. V.; Weng, F. B.; Kuo, T. W.; Huang, Z. M.; Su, A. Design and Performance Evaluation of a PEM Fuel Cell - Lithium Battery-Supercapacitor Hybrid Power Source for Electric Forklifts. *Int. J. Electrochem. Sci.* **2016**, *11* (12), 10449–10461.

(15) San Martin, J. I.; Zamora, I.; San Martin, J. J.; Aperribay, V.; Torres, E.; Eguia, P. Influence of the Rated Power in the Performance of Different Proton Exchange Membrane (PEM) Fuel Cells. *Energy* **2010**, *35* (5), 1898–1907.

(16) Mann, R. F.; Amphlett, J. C.; Hooper, M. a. I.; Jensen, H. M.; Peppley, B. a.; Roberge, P. R. Development and Application of a Generalised Steady-State Electrochemical Model for a PEM Fuel Cell. *J. Power Sources* **2000**, *86* (1–2), 173–180.
(17) Soloveichik, G. L. Liquid Fuel Cells. *Beilstein J. Nanotechnol.* **2014**, *5* (1), 1399–1418.
(18) Zhao, G.; Stuart, E. J. E.; Pumera, M. Enhanced Diffusion of Pollutants by Self-Propulsion. *Phys. Chem. Chem. Phys.* **2011**, *13* (28), 12755.
(19) Granot, E.; Filanovsky, B.; Presman, I.; Kuras, I.; Patolsky, F. Hydrazine/air Direct-Liquid Fuel Cell Based on Nanostructured Copper Anodes. *J. Power Sources* **2012**, *204*, 116–121.
(20) Kaladevi, G.; Meenakshi, S.; Pandian, K.; Wilson, P. Synthesis of Well-Dispersed Silver Nanoparticles on Polypyrrole/Reduced Graphene Oxide Nanocomposite for Simultaneous Detection of Toxic Hydrazine and Nitrite in Water Sources. *J. Electrochem. Soc.* **2017**, *164* (13), B620–B631.
(21) Wang, M.; Wang, C.; Wang, G.; Zhang, W.; Bin, F. Synthesis of MnO2/MWNTs Nanocomposites Using a Sonochemical Method and Application for Hydrazine Detection. *Electroanalysis* **2010**, *22* (10), 1123–1129.
(22) Cui, L.; Peng, Z.; Ji, C.; Huang, J.; Huang, D.; Ma, J.; Zhang, S.; Qian, X.; Xu, Y. Hydrazine Detection in the Gas State and Aqueous Solution Based on the Gabriel Mechanism and Its Imaging in Living Cells. *Chem. Commun.* **2014**, *50* (12), 1485–1487.
(23) Xu, W. Z.; Liu, W. Y.; Zhou, T. T.; Yang, Y. T.; Li, W. A Novel Fluorescein-Based “turn-On” Probe for the Detection of Hydrazine and Its Application in Living Cells. *Spectrochim. Acta - Part A Mol. Biomol. Spectrosc.* **2018**, *193*, 324–329.
(24) Lv, H.; Sun, H.; Wang, S.; Kong, F. A Novel Dicyanoisophorone Based Red-Emitting Fluorescent Probe with a Large Stokes Shift for Detection of Hydrazine in Solution and Living Cells. *Spectrochim. Acta - Part A Mol. Biomol. Spectrosc.* **2018**, *196*, 160–167.
(25) Asazawa, K.; Yamada, K.; Tanaka, H.; Oka, A.; Taniguchi, M.; Kobayashi, T. A Platinum-Free Zero-Carbon-Emission Easy Fuelling Direct Hydrazine Fuel Cell for Vehicles. *Angew. Chemie - Int. Ed.* **2007**, *46* (42), 8024–8027.
(26) Sanjay, K. S.; Zhang, X. B.; Xu, Q. Room-Temperature Hydrogen Generation from Hydrous Hydrazine for Chemical Hydrogen Storage. *J. Am. Chem. Soc.* **2009**, *131* (29), 9894–9895.
(27) Tamura, K. Exhaust Gas Compositions and Fuel Efficiencies of Hydrazine-Air Fuel Cells. *J. Electrochem. Soc.* **1976**, *123* (6), 776.
(28) Qian, W.; Wilkinson, D. P.; Shen, J.; Wang, H.; Zhang, J. Architecture for Portable Direct Liquid Fuel Cells. *J. Power Sources* **2006**, *154* (1), 202–213.
(29) Serov, A.; Kwak, C. Direct Hydrazine Fuel Cells: A Review. *Appl. Catal. B Environ.* **2010**, *98* (1–2), 1–9.
(30) Yin, W.X., Li, Z.P., Zhu, J.K., and Qin, H.Y. (2008). Effects of NaOH addition on performance of the direct hydrazine fuel cell. J. Power Sources 182, 520–523.

(31) Yu, X.; Ye, S. Recent Advances in Activity and Durability Enhancement of Pt/C Catalytic Cathode in PEMFC. Part II: Degradation Mechanism and Durability Enhancement of Carbon Supported Platinum Catalyst. *J. Power Sources* **2007**, *172* (1), 145–154.
(32) Sharma, S.; Ganguly, A.; Papakonstantinou, P.; Miao, X. Supporting Information Rapid Microwave Synthesis of CO Tolerant Reduced Graphene Oxide – Supported Platinum Electrocatalysts for Oxidation of Methanol. *Mater. Res.* **2010**, 1–9.
(33) Wang, J.; Yin, G.; Shao, Y.; Zhang, S.; Wang, Z.; Gao, Y. Effect of Carbon Black Support Corrosion on the Durability of Pt/C Catalyst. *J. Power Sources* **2007**, *171* (2), 331–339.
(34) Roen, L.M., Paik, C.H., and Jarvi, T.D. (2004). Electrocatalytic Corrosion of Carbon Support in PEMFC Cathodes. Electrochem. Solid-State Lett. 7, A19.
(35) Tang, H., Qi, Z., Ramani, M., and Elter, J.F. (2006). PEM fuel cell cathode carbon corrosion due to the formation of air/fuel boundary at the anode. J. Power Sources 158, 1306–1312.
(36) N. Elgrishi, K.J. Rountree, B.D. McCarthy, E.S. Rountree, T.T. Eisenhart, J.L. Dempsey, A Practical Beginner's Guide to Cyclic Voltammetry, J. Chem. Educ. 95 (2018) 197–206.
(37) Denuault, G.; Mirkin, M. V.; Bard, A. J. Direct Determination of Diffusion Coefficients by Chronoamperometry at Microdisk Electrodes. *J. Electroanal. Chem.* **1991**, *308* (1–2), 27–38.
(38) Bhat, Z. M.; Thimmappa, R.; Devendrachari, M. C.; Shafi, S. P.; Aralekallu, S.; Kottaichamy, A. R.; Gautam, M.; Thotiyl, M. O. A Direct Alcohol Fuel Cell Driven by an Outer Sphere Positive Electrode. *J. Phys. Chem. Lett.* **2017**, *8* (15), 3523–3529.
(39) Klingler, R. J.; Kochi, J. K. Electron-Transfer Kinetics from Cyclic Voltammetry. Quantitative Description of Electrochemical Reversibility. *J. Phys. Chem.* **1981**, *85* (12), 1731–1741.
(40) Muhammad, H.; Tahiri, I. A.; Muhammad, M.; Masood, Z.; Versiani, M. A.; Khaliq, O.; Latif, M.; Hanif, M. A Comprehensive Heterogeneous Electron Transfer Rate Constant Evaluation of Dissolved Oxygen in DMSO at Glassy Carbon Electrode Measured by Different Electrochemical Methods. *J. Electroanal. Chem.* **2016**, *775*, 157–162.
(41) Stuart, B. H. *Infrared Spectroscopy: Fundamentals and Applications*; 2004; Vol. 8.
(42) Agilent Te. UV-Visible Spectroscopy. *R. Soc. Chem.* **2000**, *Agilent Te*, 22.
(43) Chen, C.; Levitin, G.; Hess, D. W.; Fuller, T. F. XPS Investigation of Nafion® Membrane Degradation. *J. Power Sources* **2007**, *169* (2), 288–295.
(44) Rosca, V.; Koper, M. T. M. Electrocatalytic Oxidation of Hydrazine on Platinum Electrodes in Alkaline Solutions. *Electrochim. Acta* **2008**, *53* (16), 5199–5205.
(45) Alberas, D.J., Kiss, J., Liu, Z.M., and White, J.M. (1992). Surface chemistry of hydrazine on Pt (111). Surf. Sci. 278, 51–61.

(46) Yamada, K., Yasuda, K., Fujiwara, N., Siroma, Z., Tanaka, H., Miyazaki, Y., and Kobayashi, T. (2003). Potential application of anion-exchange membrane for hydrazine fuel cell electrolyte. Electrochem. commun. 5, 892–896.
(47) Ojeda, J.; Arrell, C. A.; Longetti, L.; Chergui, M.; Helbing, J. Charge-Transfer and Impulsive Electronic-to-Vibrational Energy Conversion in Ferricyanide: Ultrafast Photoelectron and Transient Infrared Studies. *Phys. Chem. Chem. Phys.* **2017**, *19* (26), 17052–17062.
(48) Alexander, J. J.; Gray, H. B. Electronic Structures of Hexacyanometalate Complexes. *J. Am. Chem. Soc.* **1968**, *90* (16), 4260–4271.